Supplementary Information (SI) for Nanoscale.
This journal is © The Royal Society of Chemistry 2024

Supporting information

Nanoscale chirality generated in zinc(II) orthophosphate clusters: Evidence by vibrational circular dichroism

Sumio Aisawa,*[a] Nami Horiguchi,[a] Chika Chida,[a] Jing Sang,[a] Hidetoshi Hirahara,[a] Akihiko Yamagishi[b] and Hisako Sato*[c]

[a] Faculty of Science and Engineering, Iwate University, 4-3-5 Morioka, Iwate 020-8551, Japan
e-mail:aisawa@iwate-u.ac.jp

[b] Faculty of Medicine, Toho University, 5-21-16 Oomori-nishi, Ota-ku, Tokyo, 143-8540, Japan

[c] Faculty of Science Ehime University, 2-5, Bunkyo-cho, Matsuyama, 790-8577, Japan
e-mail: sato.hisako.yq@ehime-u.ac.jp

Contents:

1. XRD patterns and FTIR spectra under various conditions of the mixing method

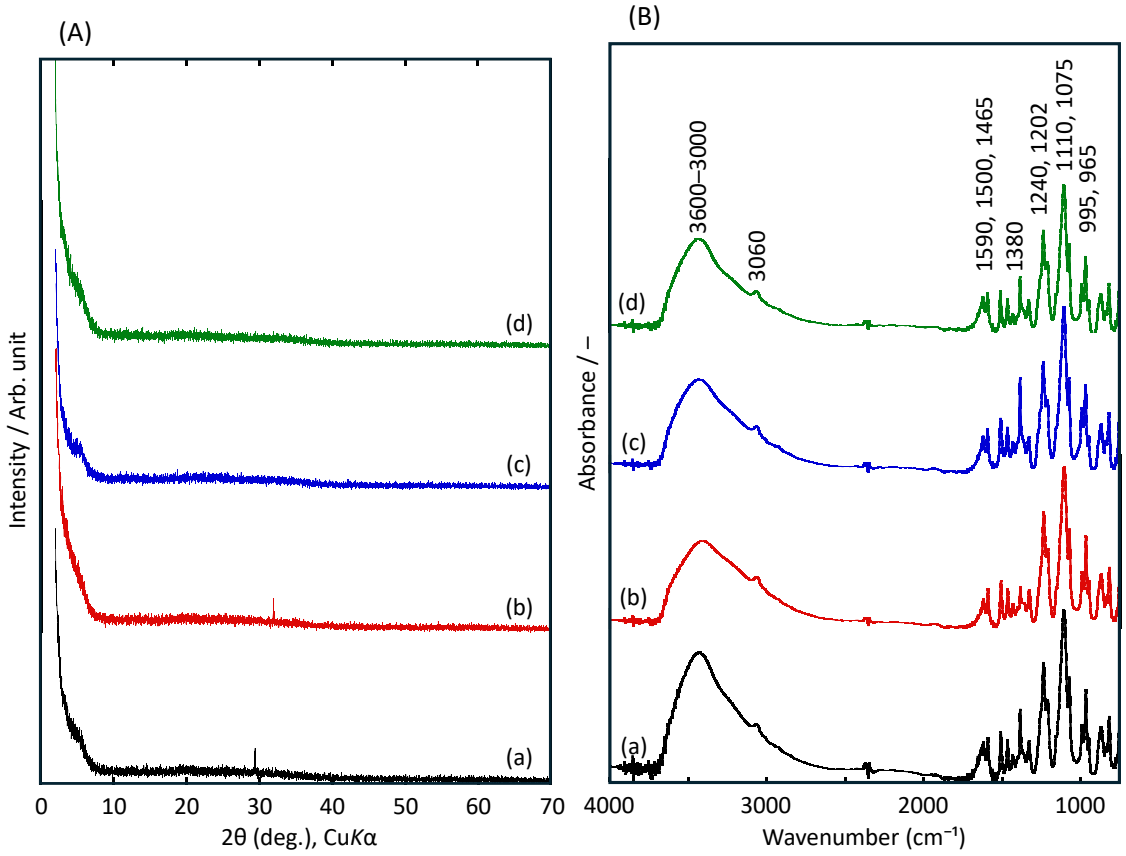

Figure S1. (A) XRD patterns and (B) FT-IR spectra of $BNDHP^{-}$/LZH, respectively: (a) *R*-$BNDHP^{-}$/LZH (pH 3.8, 40°C), (b) *S*-$BNDHP^{-}$/LZH (pH 3.8, 40°C), (c) *R*-$BNDHP^{-}$/LZH (pH 3.8, 60°C) and (d) *S*-$BNDHP^{-}$/LZH (pH 3.8, 60°C).

2. TG/DTA curves of under various conditions of mixing conditions

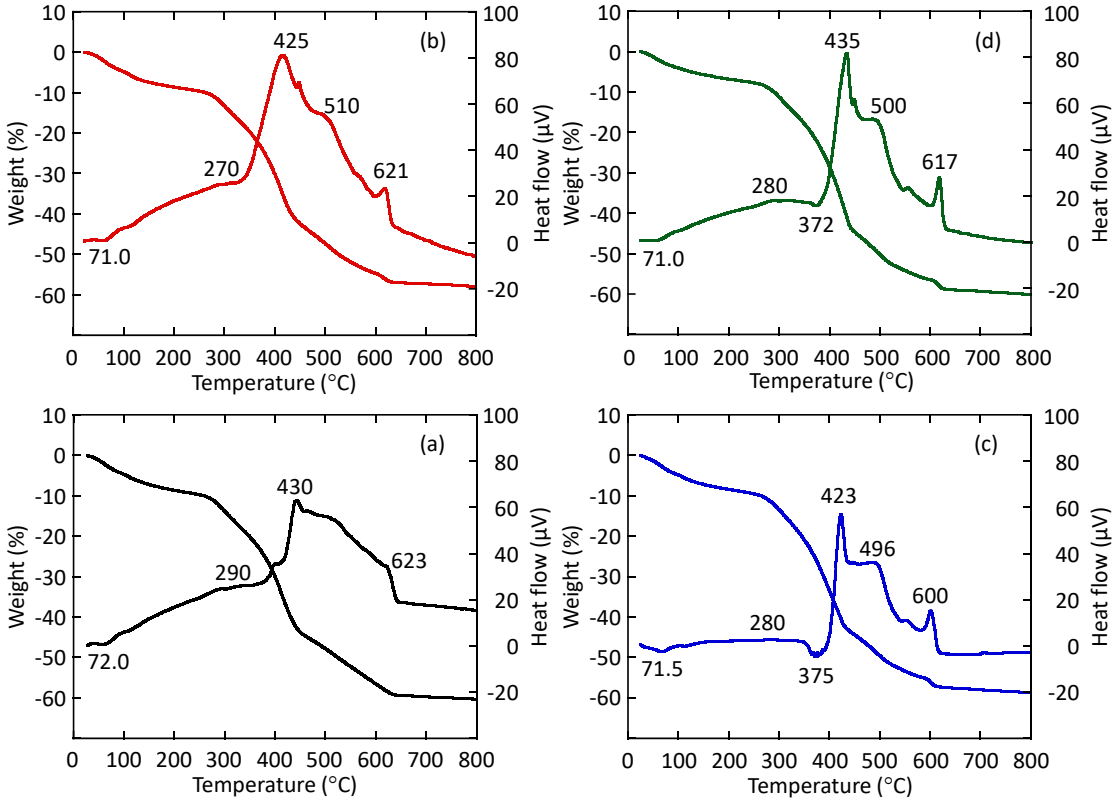

Figure S2. TG/DTA curves of (a) *R*-BNDHP$^-$/LZH (pH 3.8, 40°C), (b) *S*-BNDHP$^-$/LZH (pH 3.8, 40°C), (c) *R*-BNDHP$^-$/LZH (pH 3.8, 60°C) and (d) *S*-BNDHP$^-$/LZH (pH 3.8, 60°C).

3. XPS spectra of *R*- or *S*-BNDHP$^-$/LZH before and after calcination at 800°C

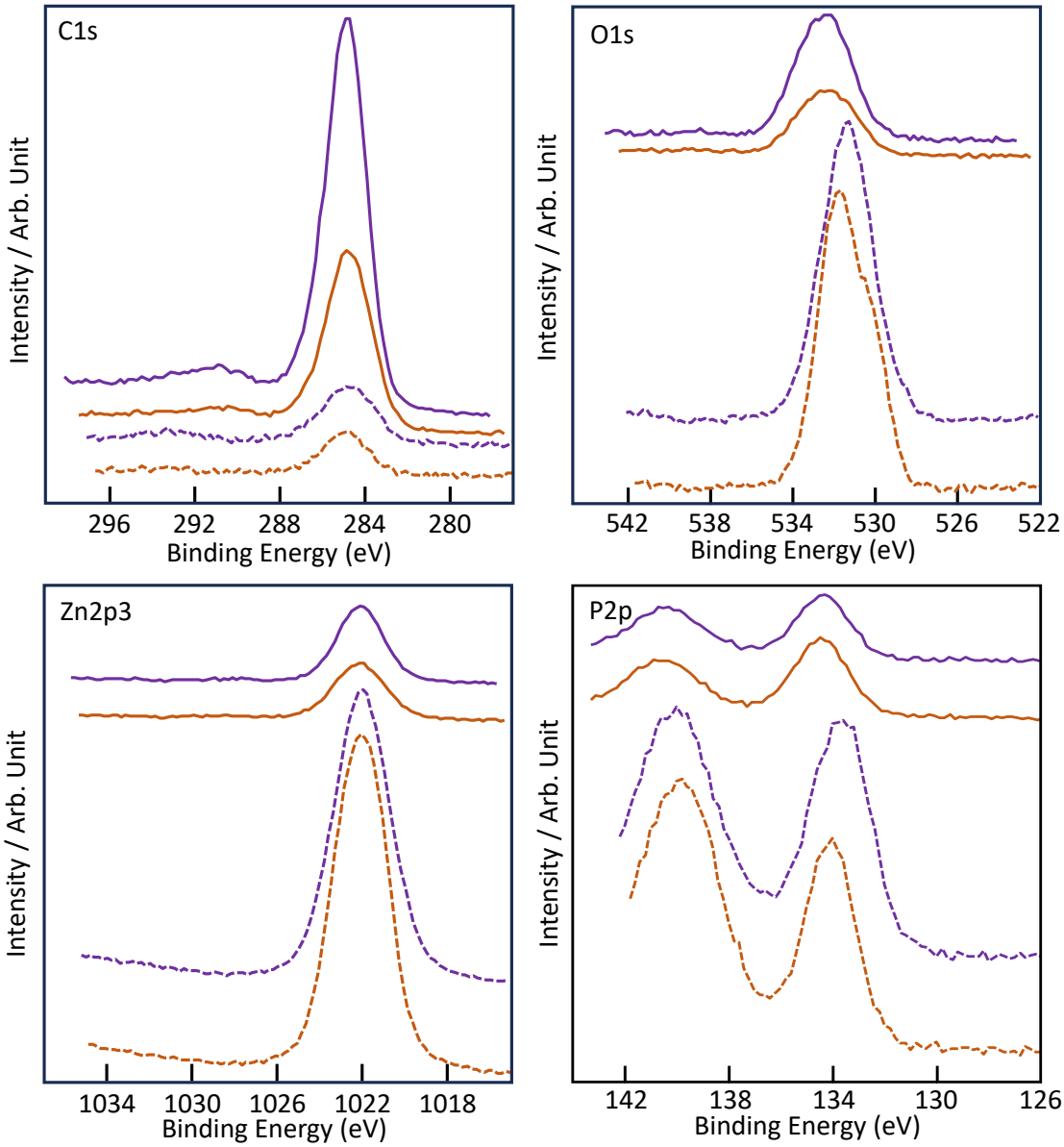

Figure S3. XPS spectra of C1s, O1s, Zn2p3 and P2p of BNDHP$^-$/LZH before and after calcination at 800°C: purple and brown lines for *R*-BNDHP$^-$/LZH and *S*-BNDHP$^-$/LZH, respectively.

4. The deconvoluted XPS spectra of *R*-BNDHP^{-}/LZH before and after calcination at 800°C

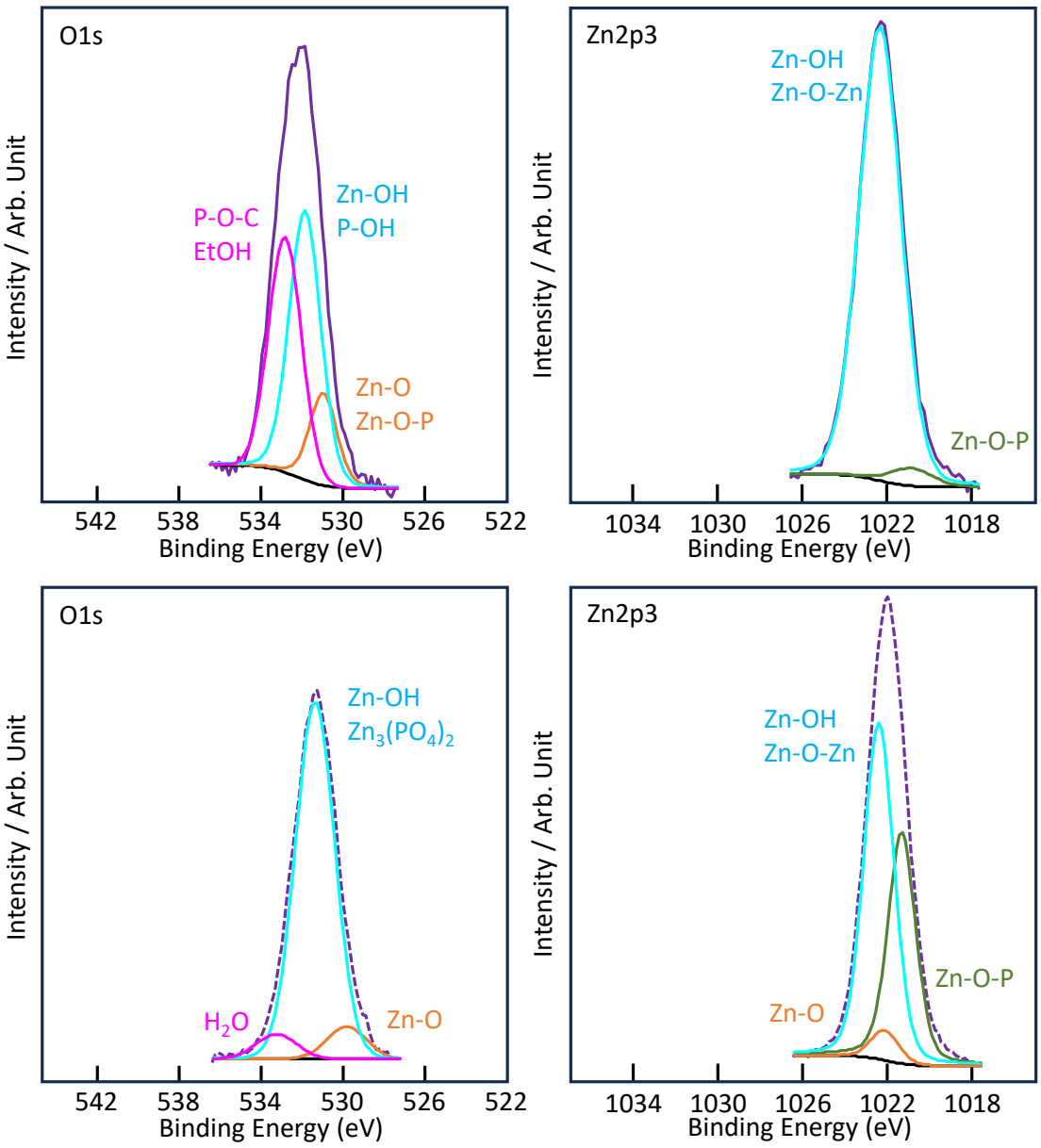

Figure S4. Deconvoluted XPS spectra of O1s (left) and Zn2p3 (right) of *R*-BNDHP^{-}/LZH before (upper part) and after (lower part) calcination at 800°C, respectively.

5. SEM images of *R*- or *S*-BNDHP$^-$/LZH before and after calcination at 800°C

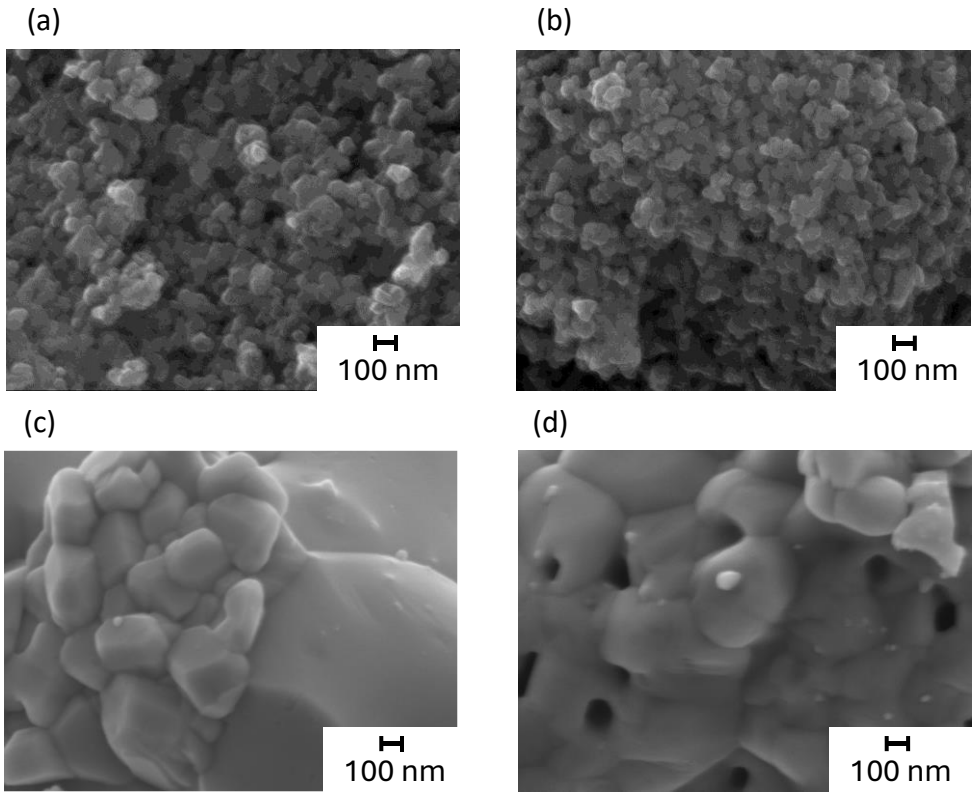

Figure S5. SEM images of (a) *R*- BNDHP$^-$/LZH (pH 5.0, 60°C), (b) *S*-BNDHP$^-$/LZH (pH 5.0, 60°C), (c) *R*-BNDHP$^-$/LZH (pH 5.0, 60°C) after calcination at 800°C and (d) *S*-BNDHP$^-$/LZH (pH 5.0, 60°C) after calcination at 800°C.

6. Experimental solid-state IR and VCD spectra of *R*- and *S*-BNDHPH

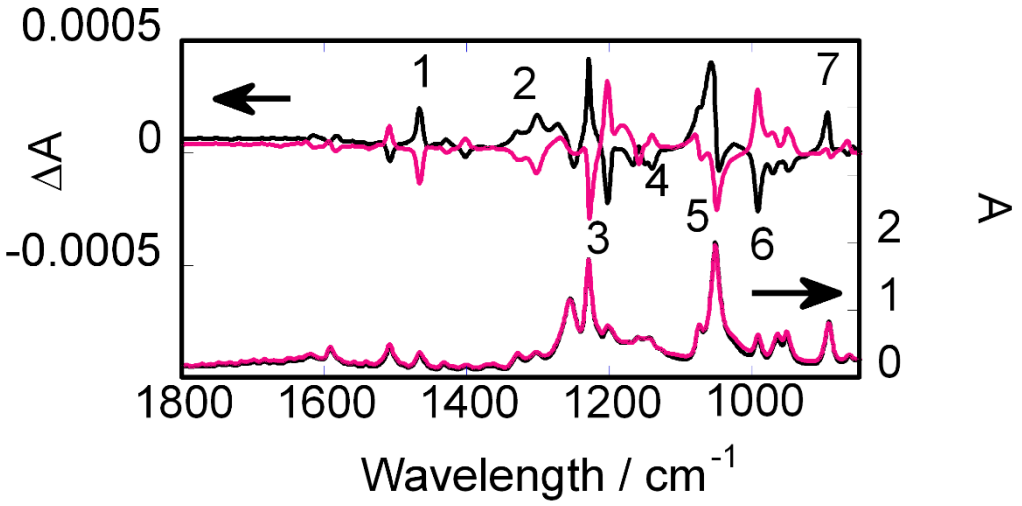

Figure S6. Experimental IR (lower) and VCD (upper) spectra: black and red curves are *R*-BNDHPH and *S*-BNDHPH of KBr pellets, respectively. Numbers show the correspondence between experimental of *R*-BNDHP-/LZH and *S*-BNDHP-/LZH in the text (Figure 4).

7. IR and VCD spectra calculated for the intercalation model

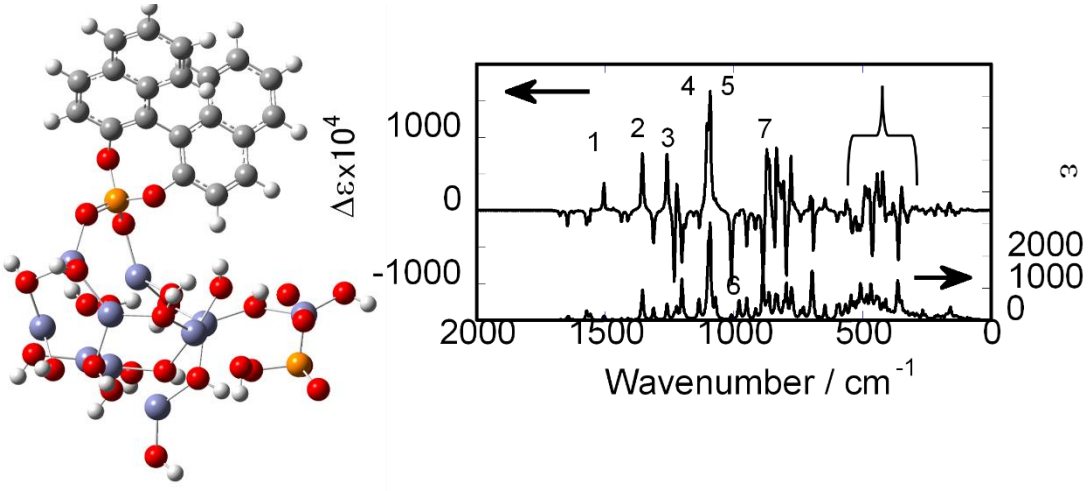

Figure S7. IR and VCD spectra calculated for the model clusters truncated LZH. *R*-BNDHP$^-$ + PO_4^- / $(Zn(OH)_2)_{10}$. The blanketed region shows the induction of chirality around Zn ions due to the chiral organic ligands.

8. IR and VCD spectra calculated for the model clusters truncated from α- or γ-$Zn_3(PO_4)_2$ crystal

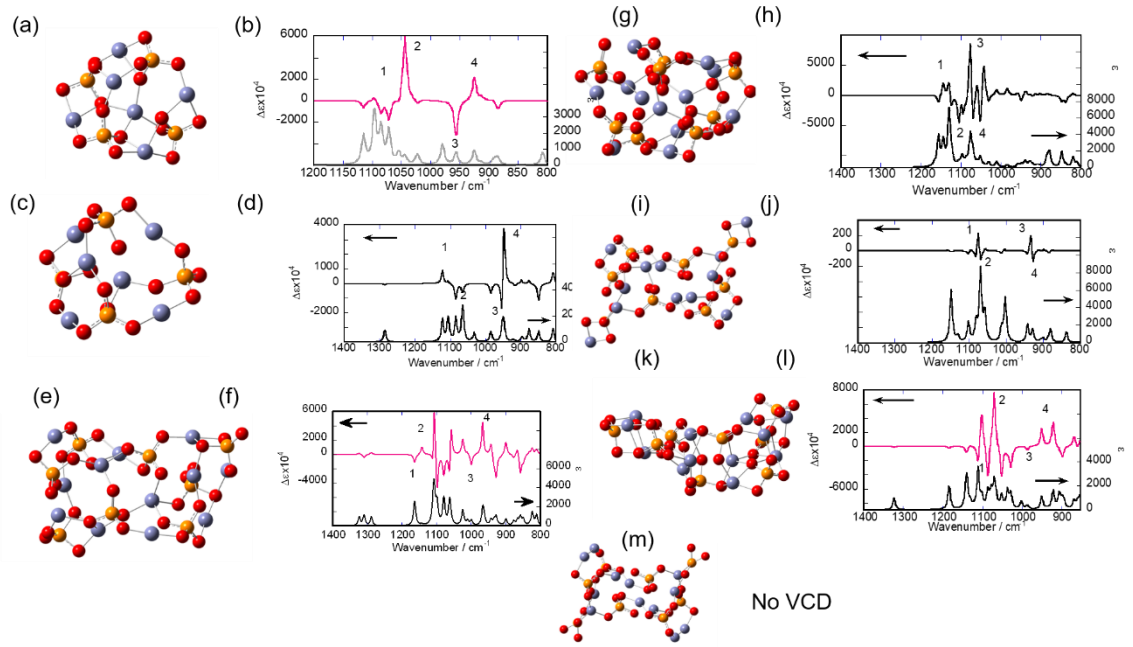

Figure S8. IR and VCD spectra calculated for the model clusters truncated from α- or γ-$Zn_3(PO_4)_2$ crystal. Red and black spectra correspond to the ones experimentally observed for the products calcinated from *S*-$BNDHP^-$/LZH and *R*- $BNDHP^-$/LZH, respectively. The clusters are constructed as below:

(a) 2 units of {$Zn_3(PO_4)_2$} from γ-$Zn_3(PO_4)_2$ crystal,

(b) IR and VCD spectra calculated for cluster (a),

(c) 2 units of {$Zn_3(PO_4)_2$} from α-$Zn_3(PO_4)_2$ crystal,

(d) IR and VCD spectra for cluster (c),

(e) 4 units of {$Zn_3(PO_4)_2$} from α-$Zn_3(PO_4)_2$ crystal (type I),

(f) IR and VCD spectra for cluster (f),

(g) 4 units of {$Zn_3(PO_4)_2$} from α-$Zn_3(PO_4)_2$ crystal (type II),

(h) IR and VCD spectra for cluster (g),

(i) 4 units of {$Zn_3(PO_4)_2$} from α-$Zn_3(PO_4)_2$ crystal (type III),

(j) IR and VCD spectra for cluster (i),

(k) 4 units of {$Zn_3(PO_4)_2$} from α-$Zn_3(PO_4)_2$ crystal (type IV),

(l) IR and VCD spectra for cluster (k).

(m) 4 units of {$Zn_3(PO_4)_2$} from α-$Zn_3(PO_4)_2$ crystal (type V). The cluster was predicted to be VCD-inactive by calculation.

9. IR and VCD spectra calculated for the model clusters composed of α-$Zn_3(PO_4)_2$ and ZnO at various ratios

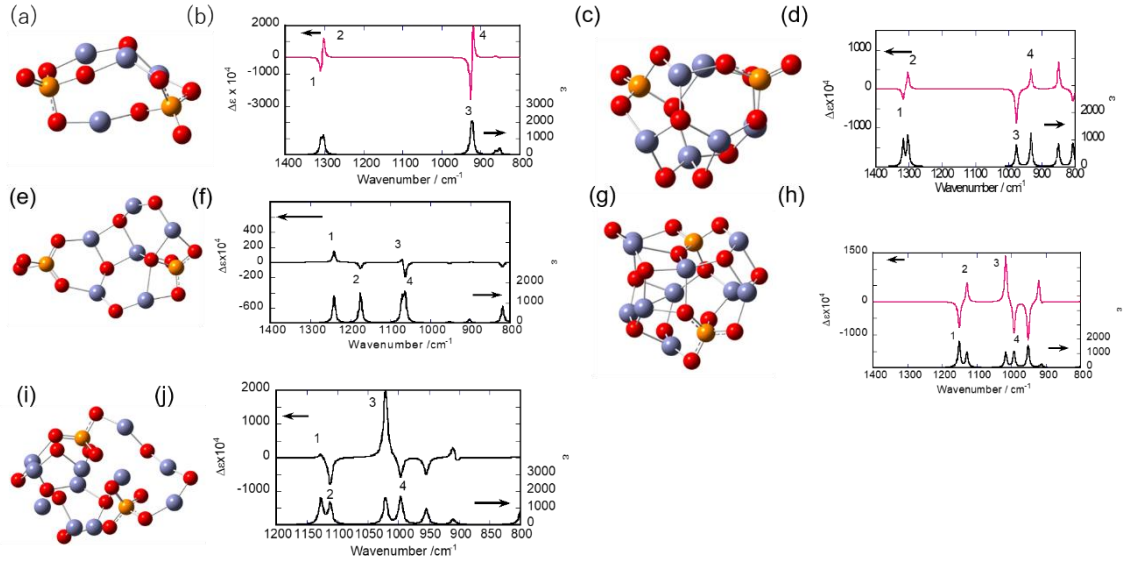

Figure S9. IR and VCD spectra calculated for the model clusters constructed from the combination of a-$Zn_3(PO_4)_2$ and ZnO at various ratios. Red and black spectra are correspondent to the ones experimentally observed for the products calcinated from *S*-$BNDHP^-$/LZH and *R*- $BNDHP^-$/LZH, respectively. The clusters were constructed according to the following combination:

(a) 1:1 of $Zn_3(PO_4)_2$ and ZnO,

(b) IR and VCD spectra calculated for cluster (a),

(c) 1:3:1 of $Zn_3(PO_4)_2$, ZnO and O (spherical type),

(d) IR and VCD spectra calculated for cluster (c),

(e) 1:3:1 of $Zn_3(PO_4)_2$, ZnO and O (planar type),

(f) IR and VCD spectra calculated for cluster (e),

(g) 1:7 of $Zn_3(PO_4)_2$ and ZnO,

(h) IR and VCD spectra calculated for cluster (g),

(i) 1:8 of $Zn_3(PO_4)_2$ and ZnO,

(j) IR and VCD spectra calculated for cluster (i).

10. VCD and IR spectra calculated for the dimer model of zinc(II) orthophosphate cluster

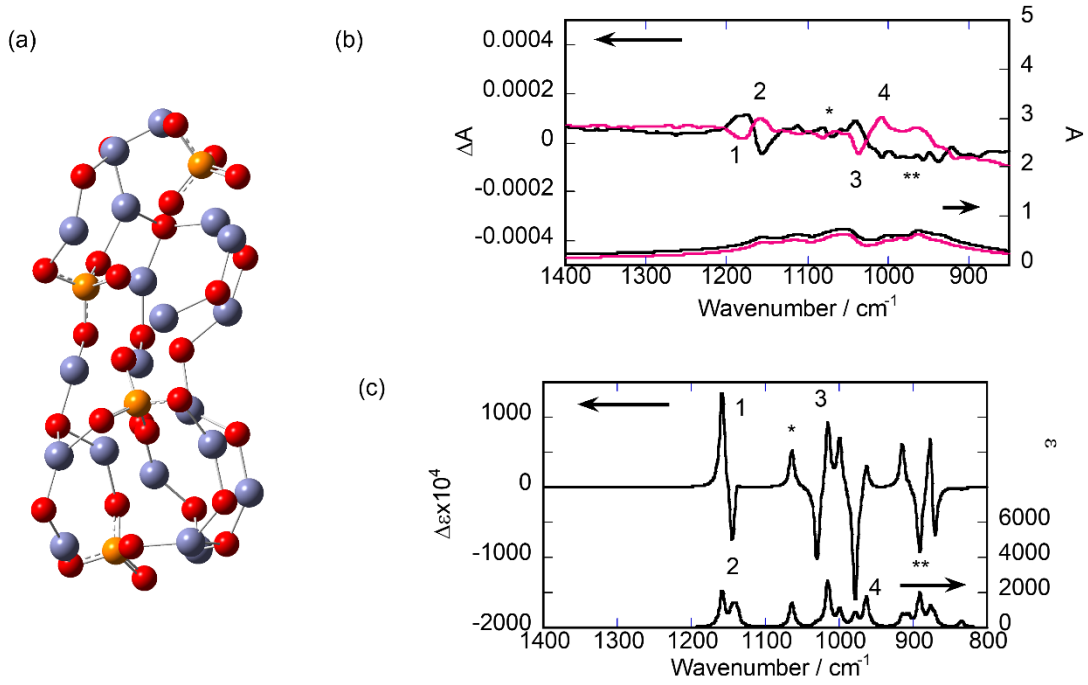

Figure S10. VCD and IR spectra calculated for a dimeric zinc(II) orthophosphate cluster. The optimized structure of a cluster is composed of two units of $\{Zn_3(PO_4)_2(ZnO)_7\}$. (a) The experimentally observed IR and VCD spectra of the calcinated samples, when the starting compounds were *R*-BNDP$^-$/LZH (red) and *R*-BNDP$^-$/LZH (black), respectively. (b) The calculated IR (lower) and VCD (lower) spectra for the dimeric model shown in (a). Two couplets (numbered as 1, 2 and 3, 4) and small peaks around 1100 cm^{-1} were reproduced as experimentally observed by the black curve in (b).